

On the Application of Integral Field Unit Design Theory for Imaging Spectroscopy

DEQING REN

National Solar Observatory, Sunspot, NM 88349; ren@nso.edu

AND

JEREMY ALLINGTON-SMITH

Astronomical Instrumentation Group, Physics Department, University of Durham, Durham DH1 3LE, UK

Received 2002 January 14; accepted 2002 April 19

ABSTRACT. Integral field spectroscopy is a powerful tool for astronomical observation, of particular importance to large telescopes. In this paper, different techniques for the design and construction of integral field units (IFUs) are described, concentrating on the use of lenslet arrays coupled to fibers. The theory of the design of the foreoptics, lenslets, and fibers is presented. The effects of the fiber oversizing and focal ratio degradation on IFU performance are described. A mathematical model is developed that can be used to calculate the optimized fiber core size according to the required coupling efficiency. A figure of merit for the IFU system is also derived, which can be used to estimate and compare the performance of different IFU systems. Finally, a design example is given to demonstrate the applications of this theory.

1. INTRODUCTION

Imaging spectroscopy produces a spectrum for every position in a field. The information content is a three-dimensional data cube, which comprises the spatial information about the observed object in two dimensions and the spectral information in the third dimension. There are two main approaches to providing this capability: integral field spectroscopy (IFS), which simultaneously gathers the three-dimensional data cube in a single integration, and scanning techniques, which use time as a third dimension.

The main scanning techniques are as follows: (1) long-slit scanning, which steps the long slit of the spectrograph across the object (e.g., McLean 1997); (2) Fabry-Perot interferometry, employing etalons with a variable cavity spacing (e.g., Boulesteix et al. 1983; Anandarao 1983; Hailash et al. 1983; Wade 1983); and (3) Fourier-transform interferometry (e.g., Connes 1970; Hall et al. 1979; Maillard & Michel 1982; Ridgway & Brault 1984; Simmons et al. 1997).

Although requiring fewer detector pixels for a given field size than IFS, these systems suffer the disadvantage that the third dimension must be obtained by scanning, requiring a greater exposure time, and are sensitive to atmospheric fluctuations during the scan, which may introduce systematic errors. In contrast, IFS provides the three dimensions simultaneously. It is most useful at high spatial resolution. Thus, IFS is particularly relevant to large telescopes that offer not only high light-gathering ability but good spatial resolution via adaptive optics or good management of the natural seeing. As a result, most of the new large telescopes will be equipped with

integral field units (IFUs), which adapt conventional types of spectrograph to IFS (Vanderriest 1998).

We discuss the main techniques of IFS in the next section. We then model the lenslet+fiber technique in § 3 and discuss the effect of nontelecentricity in § 4. The next three sections deal with the optical efficiency of the system, via a discussion of the principle of light coupling, the characteristics of the key components, and calculations of the fiber-coupling efficiency. In § 8, we discuss the appropriate figure of merit to be employed, while § 9 gives a practical example of the application of this theory.

2. IFS TECHNIQUES

There are three major IFS techniques (Allington-Smith & Content 1998): lenslets, fibers, and image slicers. The most efficient type of fiber system uses lenslets coupled to the fibers and is denoted as “lenslets+fibers” in Figure 1, which shows the different techniques schematically.

2.1. Lenslets

The field is divided into numerous small segments by a microlens array. The resultant pupil images are then dispersed by a conventional spectrograph (Courtès 1982; Bacon et al. 1995). The spectrograph output contains the individual spectra spread over the field, necessitating an adjustment to the dispersion direction to avoid overlaps. This also places limits on the length of spectrum and results in relatively inefficient use of the detector since clear gaps must be provided between adjacent spectra to avoid cross-talk. However, the system is

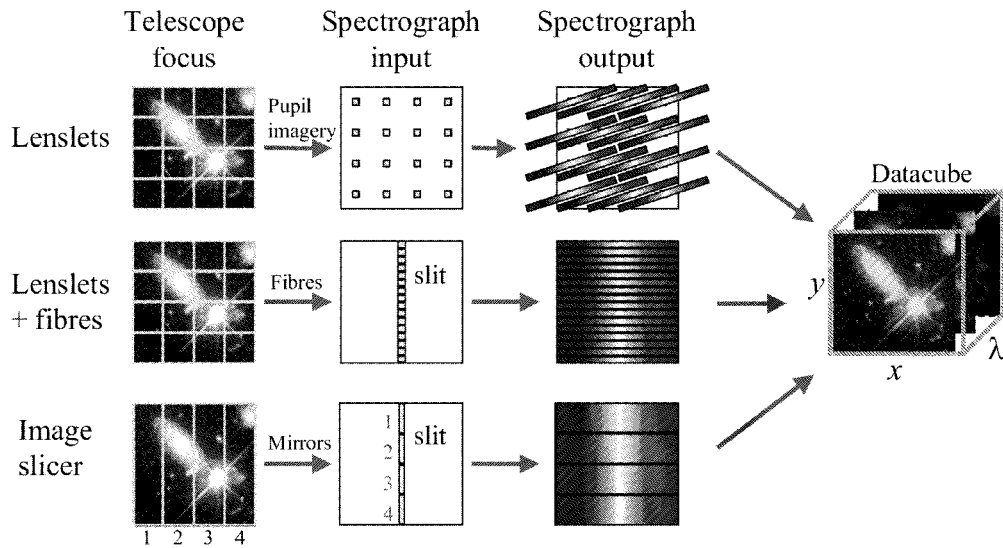


FIG. 1.—Schematic of different techniques of integral field spectroscopy.

relatively simple since it avoids the use of fibers and allows a large number of spatial samples to be obtained, providing that only limited spectral information is required. A recent example is SAURON (Bacon et al. 2001). Another is given by Herbst (1998), which is a simple system that can work at cryogenic temperature, making it suitable for infrared astronomy.

2.2. Lenslets+Fibers

An array of fibers can be used to divide the field into small pieces and then reformat the two-dimensional field into a one-dimensional strip that acts as the entrance aperture of a conventional spectrograph. Examples include SILFID at the Canada-France-Hawaii Telescope (Vanderriest 1980), the ARGUS mode of ALBIREO (Herpe et al. 1998), INTEGRAL at the William Herschel Telescope (Arribas et al. 1998), and an IFU for the Hobby-Eberly Telescope (Bershady et al. 1998). However, this technique suffers from two disadvantages. First, the filling factor is limited by the inactive parts of the fibers—the cladding and buffer that surround the active core—and the fact that round fibers cannot fill a two-dimensional region completely. Second, efficient transmission along the fibers requires an input focal ratio faster than $\sim F/5$. This is because of the nonconservation of etendue known as focal ratio degradation (FRD; e.g., Carrasco & Parry 1994), which results in the beam being faster at the output than at the input. This represents an increase in entropy and hence a unrecoverable loss of information. This focal ratio is faster than those provided by most telescopes, hence it is necessary to adapt the focal ratio with auxiliary optics.

These problems can be overcome by coupling the fibers to an array of lenslets so that each lenslet produces a small pupil

image on the fiber core, avoiding light loss due to the inactive parts of the fiber while at the same time speeding up the beam that enters the fiber. Thus, the filling factor can be increased to nearly 100% while simultaneously minimizing FRD. At the output of the fibers, a linear microlens array can be used to convert the light to a suitable focal ratio that is consistent with an existing spectrograph. The effect of FRD in this case is to increase the size of the pseudoslit, which results in a loss of spectral resolution as the effective slit width is increased. However, the output beam can be adapted by the output lenslet to avoid vignetting at the spectrograph pupil stop, thereby maximizing throughput. Without output lenslets, the spectrograph optics must be oversized to accept the fast output beam or the throughput will be reduced.

This technique requires high-quality microlens arrays and accurate registration between fibers and microlenses. However, high-quality microlens arrays and precision fiber bundles are available commercially (Lee et al. 2001; Ren 2001). Fiber-lenslet IFUs have been used so far in the visible and J and H bands of the near-infrared where cryogenic cooling is not necessary, but Haynes et al. (2000) and Tecza & Thatte (1998) have demonstrated the possibility of using this approach in cryogenic environments.

This technique is nearly optimal in terms of its efficient use of the detector. Because the spectra are aligned in wavelength, the images formed by each fiber at the slit can be allowed to overlap, since this does not mix information at different wavelengths. Of course, overlaps will affect the spatial resolution. This is discussed in depth by Allington-Smith & Content (1998), who show that modest overlapping has only a small effect on spatial resolution while allowing a large increase in

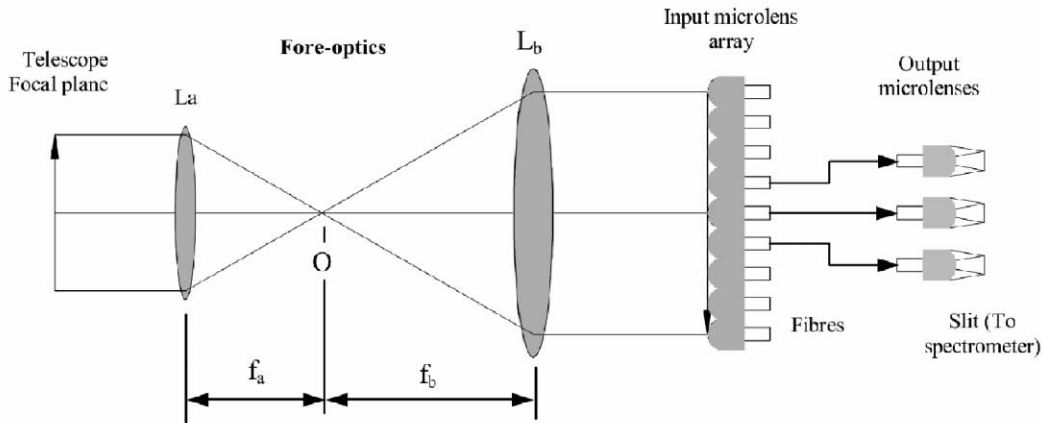


FIG. 2.—Schematic of lenslet+fiber+lenslet IFU system. For clarity, only chief rays are shown in the foreoptics. Note that the chief rays are parallel to the optical axis after the foreoptics; this means that the sky image on the input microlens front surface is telecentric.

the number of spatial samples, thus increasing the overall performance of the system.

Examples include the IFU of the GEMINI Multi-Object Spectrograph (Allington-Smith et al. 2002), a wide-field IFU for the VLT's VIMOS (Prieto et al. 1998), the AOB OSIS Infrared Fiber Unit (Guérin 1998), and SMIRFS-IFU at UKIRT (Haynes & Allington-Smith 1998).

2.3. Image Slicer

This divides the field into a number of one-dimensional slices, which are then rearranged, end to end, to form the spectrograph slit. This can be done using only mirrors and so may be conveniently employed in cryogenic environments. First proposed by Bowen (1938; see also Pierce 1965), it was developed for infrared astronomy by Weitzel et al. (1996). Their 3D instrument used sets of plane mirrors. To make this type of system more compact and easier to adapt to spectrographs designed primarily for conventional slit spectroscopy, the Advanced Image Slicer (AIS; Content 1997) was developed.

The spherical surfaces of the AIS are most conveniently made by diamond-turning a suitable metal such as aluminum. This also reduces problems of thermal stress if the mounts are made from the same material. However, diamond turning may not provide sufficiently good surface finish for use at visible wavelengths, which is why image slicers have so far been used mostly at longer wavelengths where these problems are reduced.

Another example of the application of this technique includes a system for the Hale 5 m telescope (Murphy, Matthews, & Soifer 1999). IFUs using the AIS principle include GNIRS (Dubbeldam et al. 2000) and NIFS (McGregor et al. 1999), both for Gemini, and design studies using this approach have been made for multiple IFS (Wright et al. 2000) and the *Next Generation Space Telescope* (Content & Allington-Smith 2000).

This technique makes the most efficient use of the detector of any of those discussed because interspectrum gaps are only needed between adjacent slices, which are relatively few in number. Another advantage is that the one-dimensional nature of the field division means that diffraction losses affect only the dispersion direction, in contrast to the other techniques where the two-dimensional nature of the field division leads to the potential for diffraction losses in both dimensions.

2.4. Relative Merits of the Different Systems

As outlined above, the lenslet+fiber and image-slicing systems are inherently more efficient than the lenslet-only technique in terms of efficient use of the available detector pixels. Furthermore, fibers without lenslets are generally less efficient in terms of throughput than fibers coupled to lenslets. Although the image-slicer technique offers the best performance in principle, it has not yet been proved to be efficient at visible wavelengths because of scattered light.

A number of recent projects involving the fiber-lenslet technique in the visible have recently been completed or are in progress, e.g., the FMOS IFU prototype (Ren 2001), GMOS-IFU (Allington-Smith et al. 2002), and an IFU for *Magellan's* IMACS instrument (J. Schmoll 2002, private communication). The rest of the paper concentrates on this technique.

3. FIBER-LENSLET MODELING

3.1. General Layout

The principle of a lenslet+fiber IFU employing lenslets at the IFU input and output is shown schematically in Figure 2. The telescope focal plane sky image is first magnified by the foreoptics. The magnified sky image is formed on the front curved surface of the input microlens. Each microlens forms a telescope pupil image on its back flat surface, where the fiber entrance is located. The input microlenses are arranged in a

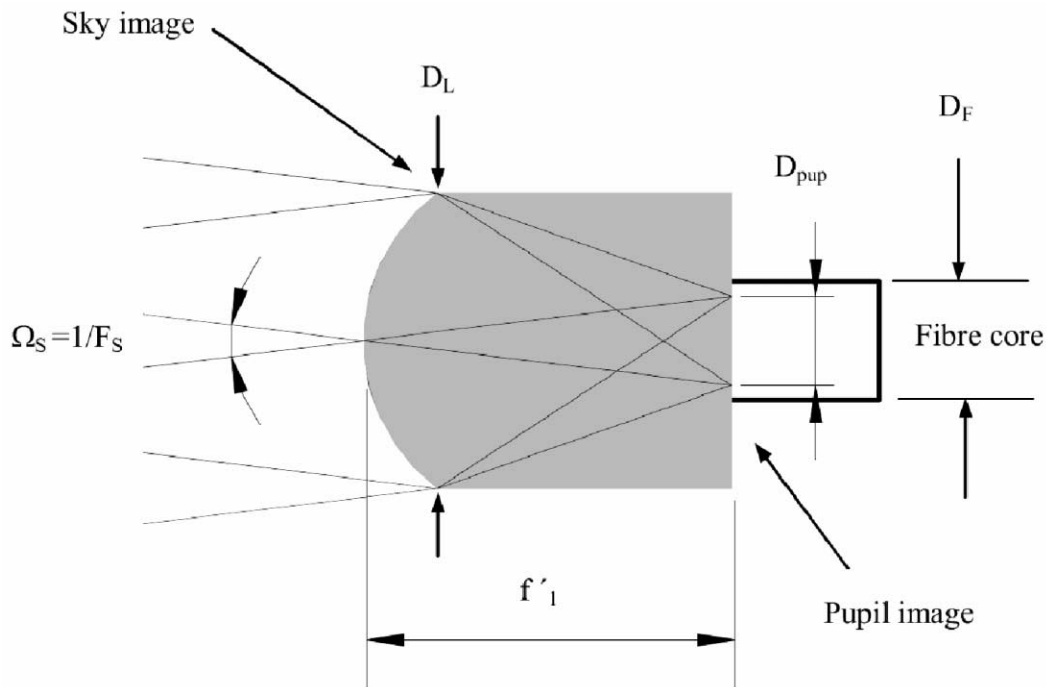


FIG. 3.—Schematic of input microlens sampling. The microlens is used to sample the sky image. The telescope pupil image is formed on its back surface. Note that the fiber core is oversized.

close-packed two-dimensional array to obtain a filling factor close to unity. At the output of the fiber, a linear microlens array is used to convert the sky image to a suitable focal ratio at the pseudoslit, which can be directly fed to a spectrograph of conventional design.

3.2. Foreoptics

In principle, one can place the input microlens array directly on the focal plane of the telescope. However, there are some advantages in having foreoptics between the telescope focal plane and the lenslet array. These include being able to use a microlens array of a suitable size and making the system from the input microlens array onward independent of the telescope and therefore potentially useful on different telescopes (Parry et al. 1997).

Its main function is to magnify the telescope focal plane image (i.e., sky image) so that it can be sampled by the input microlens array. The magnified sky image on the microlens surface must be telecentric in order to avoid pupil image shift on the microlens, which may result in light loss that varies across the field (see § 4 for further details).

In Figure 2, the sky image on the telescope focal plane is magnified by lenses L_a and L_b . In order to keep the magnified sky image telecentric, lens L_a needs to form a telescope pupil image at the object space focal point O of lens L_b in either case, i.e., for both telecentric and nontelecentric images on the telescope focal plane. In the case that the telescope focal plane

image is telecentric or the telescope exit pupil is very distant, the lateral magnification is given by

$$M = \frac{f_b}{f_a} = \frac{F_s}{F_{tel}}, \quad (1)$$

where F_s is the focal ratio of the sky image on the microlens after the foreoptics and F_{tel} is the focal ratio of sky image on the telescope focal plane.

Another advantage of telecentricity is that the magnification M is independent of the distance between the object (here it is telescope focal plane) and the foreoptics. Conventional optical systems produce images with higher magnification when the object is closer to the lens. A telecentric system acts as if it has an infinite focal length. An object moved from far away to near the optical system goes into and out of sharp focus, but its image size is constant.

3.3. Input Lenslets

The function of the input lenslets is to sample the sky image and project the telescope pupil image onto their back surfaces where the fiber entrances are located. The fibers can be fed with a fast beam in order to reduce FRD. The microlenses form a two-dimensional contiguous array with $\sim 100\%$ filling factor.

In Figure 3, assume that the microlens refractive index is n_1 and focal lengths are f_1 and f'_1 in air and in the refractive medium, respectively, so that $f_1 = f'_1/n_1$. The microlens thick-

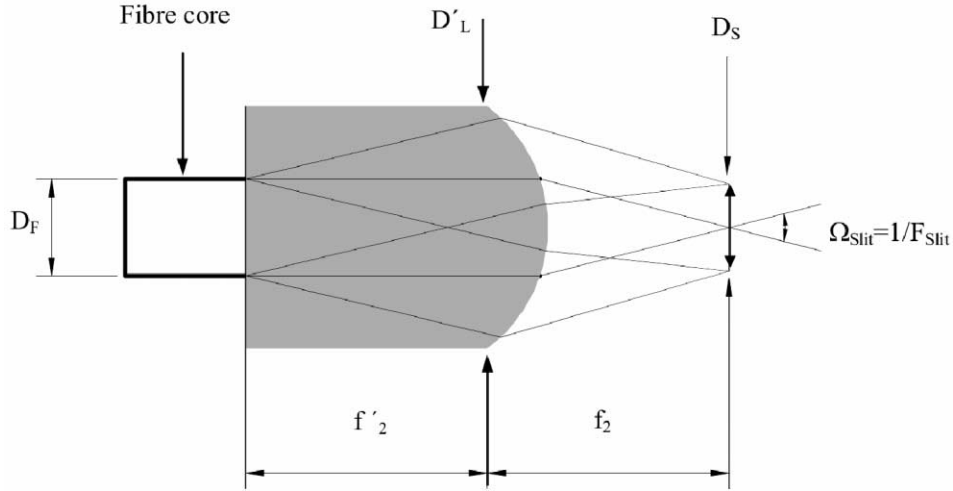


FIG. 4.—Schematic of output microlens. The microlens output focal ratio can be converted to a suitable value for an existing spectrograph. Note that the pseudoslit image is telecentric.

ness is 1 focal length in the medium. The telescope pupil image size on the fiber entrance is

$$D_{\text{pup}} = \frac{f_1}{F_s} \quad (2)$$

The focal ratio of the pupil image at the fiber entrance in air is

$$F_{\text{pup}} = \frac{f_1}{D_L} \quad (3)$$

From equations (1)–(3), the image size of the telescope pupil projected onto the fiber input entrance is

$$D_{\text{pup}} = \frac{F_{\text{pup}}}{F_s} D_L = \frac{D_{\text{samp}} F_{\text{pup}}}{F_{\text{tel}}}, \quad (4)$$

where D_{samp} is the diameter of the microlens projected on the telescope focal plane. For optimal sampling, at least two microlenses are needed to sample the FWHM of the seeing.

From equation (4), it is evident that the foreoptics has no effect on the pupil image size projected onto the fiber entrance. From equation (3), it is also obvious that the pupil image focal ratio is decided only by the microlens. One can place the microlens directly at the telescope focal plane, and the pupil image size is the same as that after the foreoptics. The function of the foreoptics is only to magnify the sky image to make it suitable for sampling by a microlens of a convenient size.

In practice, the fiber core can be oversized to match the pupil image, which may be aberrated or displaced because of an error in the fiber-lenslet registration. For a fiber with a diameter of

D_F , the oversizing factor is defined as

$$K_{\text{pup}} = \frac{D_F}{D_{\text{pup}}} \quad (5)$$

3.4. Output Lenslet

The output microlens has two functions. First, to convert the pupil image to the sky image at the pseudoslit, and second, to convert the focal ratio to a suitable value for the spectrograph. Even if a spectrograph is designed specifically for the IFU, there may be reasons (for example, cost) that may restrict the choice of design parameters. This is an important advantage of a lenslet+fiber+lenslet design compared to other kinds of IFU systems.

The fiber output end is shown in Figure 4. The telescope pupil image is at the fiber output end, which is transferred from the fiber entrance. At the fiber output, the chief ray is perpendicular to the end face at every point for the pupil image and the pupil image is telecentric so that the sky image is at infinity. The infinite sky image is converted to a real image at a distance f_2 , 1 focal length in air after the microlens, where the pseudoslit is located. The microlens thickness of 1 focal length in the medium f'_2 ensures that the sky image at the pseudoslit is also telecentric. More details about the advantages of this arrangement are given in § 5.

The focal ratio at the pseudoslit can be expressed as

$$F_{\text{slit}} = \frac{f_2}{D_F}, \quad (6)$$

where $f_2 = f'_2/n_2$.

After the fiber core size is determined by adjusting the D_F microlens focal length, the focal ratio at the pseudoslit can be adjusted to match the spectrograph. Because of the fiber scrambling, the output should be well defined in terms of its angular distribution. This well-defined beam is then fed to a spectrograph and results in no loss of throughput.

It needs to be noted that the focal ratio at the slit is decided only by the fiber core size and the output microlens focal length. Fiber FRD has no effect on it. This means that fiber FRD introduces no vignetting at the spectrograph, and there is no light loss if an output microlens of the correct size is used.

Assume that fiber FRD is defined by a constant

$$K_F = \frac{F_{\text{pup}}}{F_o}, \quad (7)$$

where F_o is the focal ratio at the fiber output end and F_{pup} is the fiber input focal ratio given by equation (3). The constant K_F is always larger than 1. It is not important how F_o is defined, provided that one controls the aperture size of the microlens (see Fig. 4), which is expressed as

$$D'_L = D_F + \frac{1}{F_o} f_2. \quad (8)$$

Equations (7) and (8) decide the actual value of F_o that the microlens system can accept. The diameter of the image formed at the pseudoslit is given by

$$D_s = \frac{f_2}{F_o} = \frac{f_2}{F_{\text{pup}}} K_F = \frac{D_F F_{\text{slit}}}{F_{\text{pup}}} K_F. \quad (9)$$

This defines the slit width. Combined with equation (5), one has

$$D_s = \frac{D_{\text{pup}} F_{\text{slit}}}{F_{\text{pup}}} K_{\text{pup}} K_F. \quad (10)$$

One can clearly see how the fiber FRD affects the performance of the spectrograph. It is evident that the slit width is decided by the FRD factor K_F and fiber oversizing factor K_{pup} . The pupil imaging optics will convert the effects of the fiber FRD into an increased image size at the slit. Both the fiber FRD and oversizing factors have the same effect of increasing the slit width, which will decrease the spectral resolution of the spectrograph. It needs to be noted that the slit size is independent of output microlens if F_{slit} is fixed or decided by an existed spectrograph. The main function of the output microlens is only to convert the pupil image to a sky image with a suitable focal ratio at the fiber output end.

3.5. Output End without Lenslets

If the fiber end is not coupled to a lenslet, the situation is simple. The bare fibers are located at the pseudoslit and directly fed to the spectrograph. The size of the pseudoslit is decided by the fiber core diameter, which can be derived by equations (4) and (5). The oversizing of fiber core will increase the pseudoslit width. The focal ratio at the pseudoslit is decided by the fiber FRD and fiber input focal ratio at the fiber input entrance. The focal ratio can be calculated according to equation (7). FRD will introduce vignetting or require that the spectrograph is oversized in aperture to accommodate the fast beam.

4. NONTELECENTRICITY

Ideally, the sky image from the telescope focal plane should be absolutely telecentric over the whole field of view. However, in practice, nontelecentricity exists for most telescopes. In this case, it will be useful to work out the allowed nontelecentric angle.

The effect of a nontelecentric sky image on the pupil position is shown in Figure 5. In Figure 5a, there is no pupil shift. This means that the center of the pupil image is on the optical axis of the microlens; i.e., the pupil image is located on the center of each microlens back surface. In Figure 5b, the pupil is shifted a distance relative to the optical axis of each microlens. The amount of the shift is different for different positions in both the telescope field of view and the IFU field of view. In the center of the telescope field, there is no pupil shift for the central microlens. However, at the edge of the IFU field, the pupil will be shifted unless the sky image is telecentric. At the edge of the telescope field, the pupil will be shifted everywhere in the IFU. Nontelecentricity will result in light loss unless the fiber cores are sufficiently oversized.

When the IFU is deployable (as for multiple IFS) and needs to move from one position to another in the telescope field, the pupil shift will change according to the field position. This effect cannot be corrected by the foreoptics. It complicates the data reduction since flat-field calibration will be required for each position of the deployed IFU. Therefore, it is highly desirable to tightly control nontelecentricity.

Nontelecentricity may be introduced by the telescope or by the IFU optics itself if the foreoptics is not a telecentric design. A foreoptic system that ensures telecentricity was discussed in § 3.2. From Figure 5b, the relationship between the nontelecentric ray angle and the pupil image shift can be derived as

$$\Delta s = f_1 \tan\left(\frac{\beta}{M}\right), \quad (11)$$

where β is the nontelecentric angle at the telescope focal plane. Given the allowed pupil shift, this equation can be used to calculate the allowed nontelecentric angle. Again, it is evident that for the same allowed pupil shift, a high magnification of

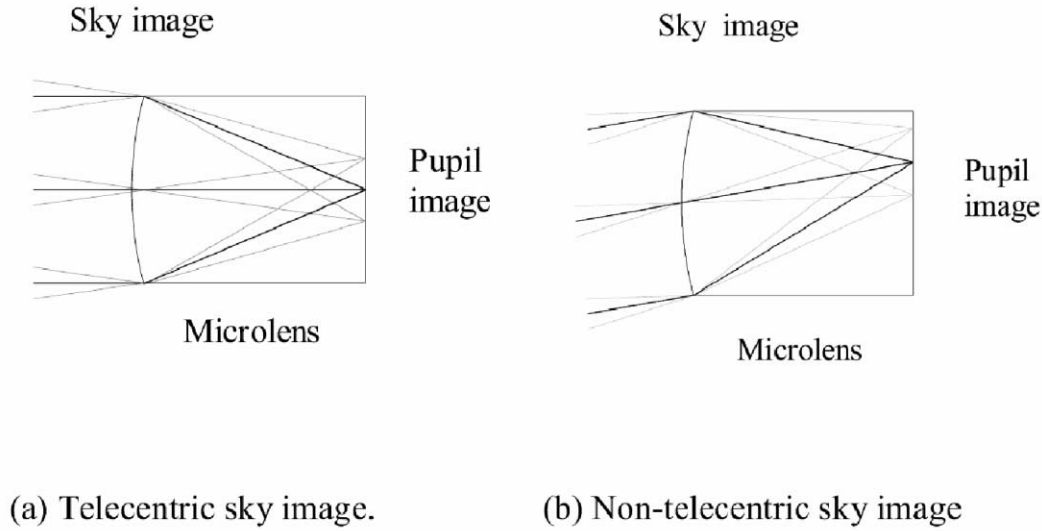


FIG. 5.—Nontelecentric sky image and pupil image shift. (a) Telecentric sky image where there is no pupil shift. (b) Nontelecentric sky image, which results in a shift of the pupil image position relative to the microlens optical axis. The thick lines are chief rays, which determine the pupil image central position on the microlens back surface. The thin lines are marginal rays, which decide the pupil image edge position.

the foreoptics allows a large nontelecentric angle in the telescope focal plane.

5. LIGHT COUPLING PRINCIPLES

Techniques for coupling light into and out of the fiber were discussed by Nicia (1981) from the point of view of communication systems and first discussed by Hill & Angel (1983) for astronomical instruments. Nicia discussed coupling light between multimode fibers using different kinds of microlenses. Hill & Angel discussed using microlenses to couple light into fibers from the telescope and then using microlenses again to couple the light to the spectrograph. However, no mathematical calculations were given concerning the design for the coupling.

The coupling efficiency can be expressed by the product

$A\Omega$ of the area of fiber core and the solid angle of emerging light. A guiding principle for using fibers is to minimize this product (Hill & Angel 1983; Brodie, Lampton, & Bowyer 1988). The smaller the product, the easier it will be to make a spectrograph with good spectral resolution and throughput.

Hill & Angel used a microlens to couple the light directly from a point source in the telescope focal plane to a fiber without using foreoptics. The configuration is shown in Figure 6. A microlens is used to couple the light from the sky image into the fiber. The distance between the sky image and the microlens is equal to the focal length of the microlens. The distance between the microlens and the fiber entrance is also arranged to be equal to its focal length. If the telescope exit pupil is infinite or very distant, the telescope exit pupil is imaged onto the fiber entrance by the microlens and the chief rays of the pupil image are parallel to the optical axis everywhere on the fiber entrance. Therefore, the $A\Omega$ product is exactly conserved. A reversed arrangement is used for the output end of the IFU (Fig. 4) to ensure that the $A\Omega$ product is exactly conserved. Another advantage is that the fiber can be fed at a fast focal ratio to reduce FRD. This method of coupling has the feature that the cone angle of the beam emerging from the fiber is not invariant, as in the simple coupling of bare fibers, but is sensitive to changes in telescope image quality. If the seeing improves, then Ω at the output is reduced, and, from equation (10), the slit becomes narrower and the spectral resolving power increases. However, this is true only for a point source. For an extended sky image, this feature does not exist.

Unfortunately, the configuration proposed by Hill & Angel cannot be used for the input of an IFU where the extended sky image needs to be sampled. For a microlens array, this con-

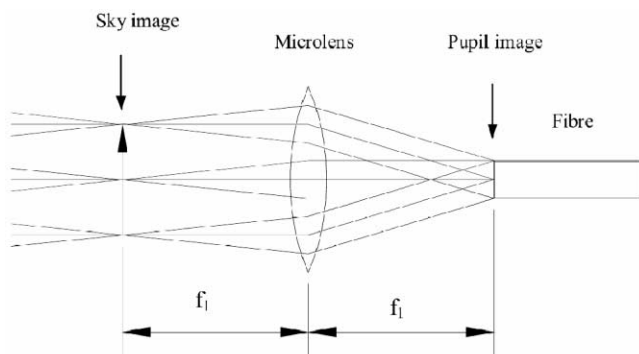


FIG. 6.—Schematic of an optical system that uses a microlens to couple the light into a fiber. In this arrangement, the chief rays of the pupil image are parallel to the optical axis everywhere on the fiber entrance and the $A\Omega$ product is exactly conserved.

figuration will introduce a blurred sky image on each microlens surface and cause cross-talk in the sampling process. The best method is to form the sky image on the curved surface of the microlens array. The aperture of each microlens can then sample the sky image accurately and, since the microlens array can have a 100% filling factor, no light is lost in the process. Meanwhile, each microlens can also image the telescope exit pupil onto its back surface.

Although this method appears to be good for the IFU, at the input end another problem appears. As the sky image is placed directly on the microlens surface, the chief rays of the pupil image are no longer parallel to the optical axis of each microlens. The angle between the chief ray and optical axis is variable. On the edge of the pupil image, one gets a maximum value of

$$\theta_{\max} = \frac{1}{F_s} = \frac{1}{MF_{\text{tel}}}, \quad (12)$$

where F_s is the focal ratio of the sky image after the foreoptics, M is the magnification of the foreoptics, and F_{tel} is the telescope focal ratio.

Because the chief ray has an extra angle on the pupil image plane, when this light is fed to a fiber it will introduce extra FRD, often known as *geometrical FRD*. From the above equation, for the IFU input microlens, this angle is decided only by the input focal ratio of the telescope sky image and the foreoptics magnification. If the beam of the telescope sky image is slow or the foreoptics has a high magnification, the geometrical FRD will be very small. As an example, if $M = 20$ and $F_{\text{tel}} = 2$, then $F_s = 40$. This beam is very slow and the geometrical FRD can be neglected, compared with the focal ratio at the fiber input, which has a typical value of F/5. It is evident that high magnification in the foreoptics will reduce the geometrical FRD.

6. FIBER AND MICROLENS PROPERTIES

The fibers used in astronomy are of the step-index type (Parry 1998). Fiber FRD has been studied and measured by several authors (Gloge 1972; Gambling, Payne, & Matsumura 1975; Heacox 1986) from different points of view. Because FRD is difficult to measure accurately and the measurement changes from fiber to fiber, the reliability of these comparisons is a problem. Even the same fiber may have different FRD if the measurement is made by a different person or if the fiber is from a different batch. Only Heacox (1986) has studied the fiber properties theoretically for the application of bare fibers to couple the light between the telescope and spectrograph.

Microbending-induced beam spreading in optical fibers was analyzed by Gloge (1972), who developed an equation to describe the distribution of optical power P in a fiber. This equation was solved by Gambling et al. (1975) in the case of a collimated input beam at incident angle θ_0 . An asymptotic form

was given by Heacox (1986), and the output angular flux distribution in the far field is approximately given by

$$P(\theta|\theta_0) \propto \exp\left[-\frac{1}{2}\left(\frac{\theta - \theta_0}{\sigma_{\text{bs}}}\right)^2\right], \quad (13)$$

where

$$\sigma_{\text{bs}} = \frac{\lambda}{d_f} \left(\frac{1}{2n} \frac{L}{L_D} + 0.19\right)^{1/2}, \quad (14)$$

where L is the fiber length, λ is the light wavelength, d_f is the fiber core diameter, n is the refractive index of the fiber core, and L_D is a constant, called the modal diffusion length, which characterizes the microbending.

From this result, Heacox derived that the change in focal ratio of the input beam is given roughly by

$$\Delta F \approx 2F^2 \sigma_{\text{bs}}, \quad (15)$$

where F is the focal ratio of the input beam.

Clearly, to reduce FRD, one must keep σ_{bs} and F small. There are some parameters that affect σ_{bs} : (1) short fiber length is helpful to reduce FRD, and (2) FRD will be more serious at long wavelength and for fibers with small core diameter. From equation (4) it is obvious that for the IFU, a fast beam will produce a small pupil size on the fiber entrance and thus need a small fiber core size. It needs to be noted that in the previous discussion, the fiber core is allowed to be oversized. This has a potential advantage to reduce the FRD.

Let us consider the input microlens (Fig. 3). The characterization of lenslets has been discussed elsewhere (Lee et al. 2001; Ren 2001). The main optical aberration is chromatic-spherical. The transverse spherical aberration (TSA) of the plano-convex microlens can be derived as (Ren 2001)

$$\text{TSA} = \frac{D_L}{16F_{\text{pup}}^2 n_1^2 (n_1 - 1)^2}. \quad (16)$$

The relationship between spherical aberration and microlens diameter is linear. Increasing the microlens size will increase the spherical aberration, which is inversely proportional to the square of the F number. Increasing the microlens diameter will increase the pitch of the microlens array, which may make the construction of the fiber bundle easier. A large diameter can also increase the filling factor if the microlenses are subject to deviations in shape at the edge of the microlens aperture because the affected regions are likely to be of fixed size (Sugai et al. 2000; Ren 2001). A good compromise for the microlens diameter is about 500 μm .

Figure 7 shows the chromatic-spherical aberration of an actual microlens optimized for the minimum chromatic-spherical aberration. The figure shows that the image quality is still diffraction-limited if the beam is slower than about F/5 for the

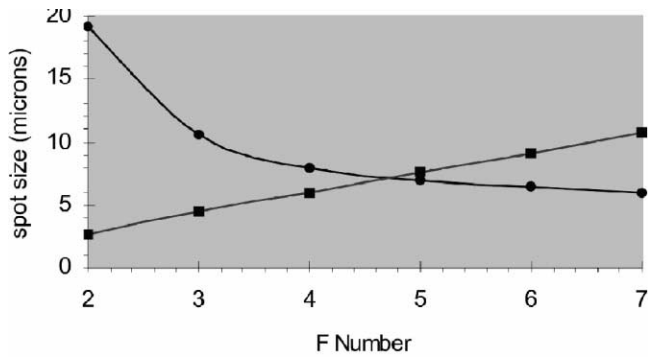


FIG. 7.—Spot size vs. focal ratio for a 500 μm diameter silica microlens over a 0.4–0.9 μm wavelength range. Circles represent chromatic-spherical aberration. Squares represent the Airy disk at the primary wavelength of 0.63 μm.

microlens. The optical material is silica, and the wavelength range is 0.40–0.9 μm. Other suitable glasses, such as BK7, have similar performance.

For a diffraction-limited microlens, the depth of focus can be expressed as

$$\Delta z = \pm 2\lambda n_1 F_{\text{pup}}^2. \tag{17}$$

Assuming that the wavelength is 0.4 μm, the depth of focus is ±10, ±19, ±29, and ±42 μm for F/3, F/4, F/5, and F/6 microlenses, respectively. The requirement that the lenslet forms an image of the telescope pupil on its back surface implies that the thickness tolerance of the microlens should be less than or equal to the depth of focus. Typically, the tolerance on the microlens array thickness is ±20 μm. From this, it is apparent that the microlens focal ratio should be no faster than F/4 in the visible wavelength range, considering the manufacturing tolerance.

Considering the properties of both fiber and microlens, the optimum situation is a focal ratio of ~F/5 and a microlens diameter of 500 μm.

7. FIBER COUPLING EFFICIENCY

For an IFU, the telescope pupil is projected by the microlens onto the fiber entrance. In this application, the scene of the telescope pupil is an extended source. Optical aberrations can be expressed as a point-spread function (PSF) consisting of a two-dimensional circularly symmetrical Gaussian function (Jacobs & Edwards 1999). The polar representation of this function is

$$G(r) = \frac{1}{2\pi\sigma^2} \exp\left(-\frac{r^2}{2\sigma^2}\right), \tag{18}$$

where σ is the standard deviation of the Gaussian function and r is the radius.

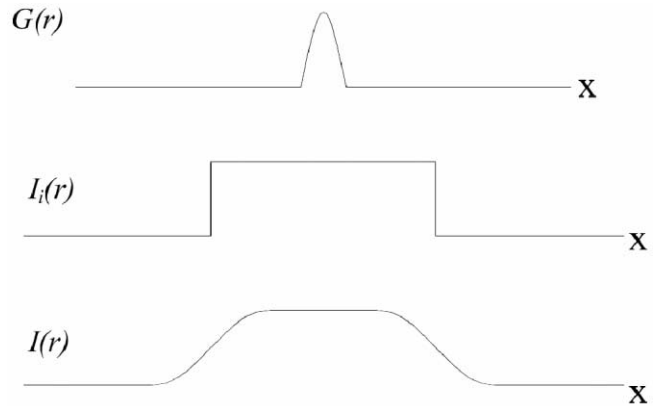


FIG. 8.—Schematic of the process by which an image is blurred by optical aberration: $G(r)$ is the PSF of the optical system, $I_i(r)$ is the perfect scene image (pupil image), and $I(r)$ is the blurred image.

Assume that the perfect pupil image has unit intensity over the whole field so it can be represented by

$$I_i(r) = \begin{cases} 1 & \text{if } |r| < d/2, \\ 0 & \text{otherwise.} \end{cases} \tag{19}$$

The process by which a perfect image is blurred by the optical aberration is shown schematically in Figure 8. The convolution of the Gaussian function with the rectangular function yields the following analytic result for the blurred image:

$$I(r) = I_i(r) \otimes G(r) = \frac{1}{4\delta} \left(\frac{2}{\pi}\right)^{1/2} \left\{ \text{erf}\left[\frac{d/2-r}{\sqrt{2}\delta}\right] - \text{erf}\left[\frac{-d/2-r}{\sqrt{2}\sigma}\right] \right\}, \tag{20}$$

where erf(x) is the error function and $I(r)$ is a circularly symmetrical function.

The coupling efficiency is defined as the ratio of the collected flux of the light when the fiber core diameter is of finite size to that when the fiber core size is infinite. It is expressed as

$$\eta(R) = \frac{F(R)}{F(\infty)}, \tag{21}$$

where $F(R)$ and $F(\infty)$ are the flux of light collected by the fiber when the fiber core radii are R and infinity, respectively.

As the irradiance profile $I(x)$ has circular symmetry, the coupling efficiency is

$$\eta(R) = \frac{\int_0^R I(r) 2\pi r dr}{\int_0^\infty I(r) 2\pi r dr}, \tag{22}$$

The function $I(r)$ can be calculated from equation (20). Some calculations and results will be discussed in a later section.

8. FIGURE OF MERIT

There are different ways to define the figure of merit for the system performance of an imaging spectrograph. A figure of merit, which was proposed by Allington-Smith & Content (1998), is given as $Q = N_{\text{spatial}} \times N_{\text{spectral}} \times \text{efficiency}$, where N_{spatial} and N_{spectral} are the numbers of independent samples in the spatial and spectral directions, respectively. Based on Jacquinot's (1954) method, a figure of merit was given by Atherton (1983) as $Q = B \times \tau \times A \times \Omega \times R \times N_{\lambda}$, where B is the source function, τ is the efficiency, A is the area of the collimated beam, Ω is the solid angle subtended by the entrance aperture, R is the resolving power, and N_{λ} is the number of parallel spectral channels, i.e., spectral multiples. Atherton used this formula to compare the performances of the imaging long-slit spectrograph, imaging Fabry Perot spectrograph, and imaging Fourier-transform spectrograph.

However, for the fiber IFU system, the situation is different. In principle, there is no limitation to the size of the field of view. The number of fibers and microlenses can be as large as possible. From the discussion in the previous sections, the performance of the IFU is determined by the fiber FRD, the actual fiber core size, and so on. The optical aberration and registration error between the fiber bundle and microlens array are included in the fiber-oversizing constant K_{pup} . If the fibers are not oversized, this will result in a light loss and low throughput. Therefore, the performance of a fiber IFU can be estimated according to a figure of merit, which is given as

$$Q = \sqrt{\frac{\Omega A}{\Omega_o A_o}} \eta, \quad (23)$$

where η is the efficiency of the IFU. This includes the reflection and transmission loss of the IFU optics and the light loss in the coupling process. The variables Ω and A are the solid angle and area of a sampling element at the telescope focal plane, respectively. The sampling element is magnified by the IFU foreoptics and sampled by a microlens and then coupled into a fiber. After this sample is output from the IFU at the pseudoslit, it is characterized by Ω_o and A_o . A perfect IFU will have a figure of merit of 100%. From equations (23), (10), and (4), the figure of merit is thus

$$Q = \frac{\eta}{K_{\text{pup}} K_f}. \quad (24)$$

This equation applies to both lenslet+fiber+lenslet and lenslet+fiber systems. Again from this equation, it is evident that the oversizing of the fiber core has the same effect as FRD on the system performance.

The IFU performance can also be estimated according to the spectral resolution of the spectrograph. For a perfect IFU, the pseudoslit width is minimized when both K_{pup} and K_f are unity. However, the slit may be broadened because of FRD or fiber

oversizing. The actual resolution of the spectrograph is (Ren 2001)

$$R = R_0 \frac{D_0}{D_s}, \quad (25)$$

where R_0 and D_0 are the nominal spectral resolution and slit width of the spectrograph, respectively, when both K_{pup} and K_f are equal to 1, and R and D_s are the actual spectral resolution and slit width of the spectrograph, respectively.

Combined with equation (10), the actual spectral resolution for an IFU with output lenslets is

$$R = \frac{R_0}{K_{\text{pup}} K_f}. \quad (26)$$

Clearly, equations (24) and (26) are consistent. For the IFU without output lenslets, the FRD has no effect on the resolution, but loss of throughput may arise due to vignetting in the spectrograph if the spectrograph is not oversized to accommodate the faster output beam. In this case, the resolving power is

$$R = \frac{R_0}{K_{\text{pup}}}. \quad (27)$$

In order to reduce K_{pup} , each fiber needs to be correctly registered with its corresponding microlens. Current microlens arrays can have a pitch accuracy of better than 1 μm , so the microlens-microlens position error is very small and the fiber-fiber position in the bundle is often the dominant source of registration error.

9. A PROTOTYPE IFU FOR FMOS

FMOS (Maihara et al. 2000) is a versatile optical and near-infrared fiber spectroscopic facility for the prime focus of the 8 m Subaru telescope, currently under construction. There is an upgrade option to use multiple deployable IFUs at the Subaru prime focus for imaging spectroscopy. As the spectrographs are located away from the prime focus, the instrument must use fibers to transfer the telescope focal image to the spectrograph slit. A prototype IFU was designed and constructed at the University of Durham (Ren 2001).

The optical layout of the IFU is shown in Figure 9. The F/2.2 beam from the telescope's primary mirror is directed into the IFU by a BK7 prism before the primary focus. An SK2 lens is glued to the prism to form a prism lens. An F5/SK2 doublet is located behind the prism lens, and a fused silica singlet is placed before the microlens array. The telescope's pupil is projected on the focal plane of the prism lens, which is also the object space focal plane of the doublet and the singlet. The pupil is then imaged at infinity by the doublet and singlet so the sky image is telecentric on the microlens front surface. The prism lens, the doublet, and the singlet comprise

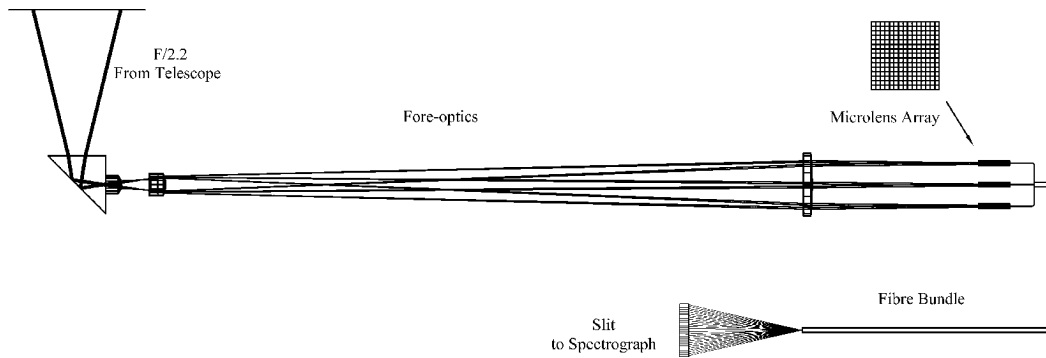


FIG. 9.—Layout of the prototype IFU proposed for FMOS.

the foreoptics of the IFU. The focal length of the doublet and singlet is 20 times that of the prism lens, so the foreoptics magnification is 20. The sky image is then sampled by a 15×15 microlens array, and the pupil image is fed onto a custom-manufactured 15×15 fiber bundle at F/5. The fiber positional accuracy at the input end of the bundle is better than $3.5 \mu\text{m}$ rms so that the microlenses and fibers are accurately registered. At the other end of the bundle, the fibers are arranged to form the long slit of a dedicated spectrograph with a nominal output focal ratio of F/5.

The IFU works in the visible ($0.45\text{--}0.9 \mu\text{m}$) and near-infrared ($0.9\text{--}1.8 \mu\text{m}$) simultaneously in order to make best use of the telescope time. The sampling increment is 0.3 for each microlens. For multiple IFS, 20 IFUs are deployed at the Subaru $30'$ diameter focal plane.

The $20 \times$ magnification results in a sampling aperture of $500 \mu\text{m}$ for each microlens. The microlens focal length is 2.8 mm , so the focal ratio of the pupil image is F/5 at the fiber input entrance. Given the allowed maximum pupil shift of $5 \mu\text{m}$, the maximum permitted nontelecentric angle is 2.1° over the whole telescope field of view (eq. [12]).

The pupil image is formed on the back surface of each

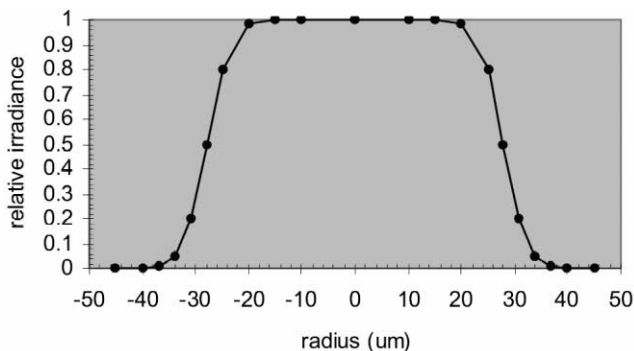


FIG. 10.—Cross-sectional profile of the pupil image irradiance of the prototype IFU. The perfect pupil image size is $d = 56 \mu\text{m}$. The rms radius of the optical aberration is $\sigma = 3.6 \mu\text{m}$. The FWHM of the profile is still about $56 \mu\text{m}$, the same as the perfect image.

microlens. In the perfect case, it would have a diameter of $d = 56 \mu\text{m}$. The optical aberration can be expressed by the rms spot radius with maximum rms radius of $\sigma = 3.6 \mu\text{m}$ over the whole field according to ray-tracing. The blurred image of the telescope pupil was calculated by equation (20). Figure 10 is the cross-section profile of the blurred pupil image of the IFU. The coupling efficiency is calculated according to equation (22), and the result is shown in Figure 11. The FWHM is almost unaffected by the blurring and is still close to $56 \mu\text{m}$.

From the calculations, some general conclusions can be drawn. When the fiber core size is the same as the perfect scene, some light may not be collected by the fiber. The fiber core needs to be oversized to ensure high coupling efficiency. The above example suggest that when the fiber core radius is oversized by σ and 2σ , about 97% and 99% of the light can be collected, respectively. If the alignment error between microlens and fiber is Δt , the fiber core radius should be between $d/2 + \sigma + \Delta t$ and $d/2 + 2\sigma + \Delta t$. For this prototype, the actual alignment error of the Δt is less than $3.5 \mu\text{m}$ rms.

Let us consider the figure of merit. The actual pupil image size is about $67 \mu\text{m}$ because of the optical aberration. The fiber core is oversized to $80 \mu\text{m}$ considering the alignment error

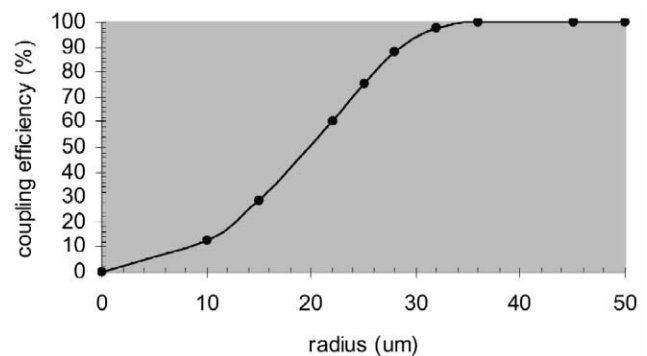


FIG. 11.—Coupling efficiency vs. fiber core radius. The coupling efficiency is 88.4% at radius $28 \mu\text{m}$, 97.5% at radius $32 \mu\text{m}$ ($d/2 + \sigma$), and 99.8% at radius $36 \mu\text{m}$ ($d/2 + 2\sigma$).

between microlenses and fibers and the available diameters of fibers, so $K_{\text{pup}} = 1.42$. The pupil image is fed to the fiber at $F/5$ (defined by two opposite corners of the microlens, which is square in this case) and emerges at $\sim F/4$ because of FRD, so the fiber FRD factor $K_F = 1.25$. If we assume that there is no light loss in the coupling process because the fiber is oversized enough to accommodate the registration error and the optical aberration, this results in $Q = 0.56\eta$ and an actual spectral resolution of $R = 0.70R_0$ according to equation (27). Thus, the fiber oversizing results in a lower spectral resolution than the nominal value.

10. CONCLUSIONS

In this paper, the use of lenslet-coupled fibers in integral field units was discussed. The function of the IFU foreoptics is to magnify the telescope focal plane image to make it suitable for sampling by the lenslets and create a telecentric sky image. The advantages of telecentric designs were demonstrated. High-magnification foreoptics can reduce the non-telecentric angle on the fiber entrance.

For IFUs, microlenses can be used to couple light into the

fibers. We showed how to design a lenslet+fiber system that can maximize the conservation of etendue (the $A\Omega$ product). It is evident that high-magnification foreoptics can reduce geometrical FRD for the input microlenses.

Fiber and microlens properties were also discussed. Fiber FRD is a function of fiber modal diffusion length, fiber core size, fiber length, and wavelength. Oversizing the fiber core may help to reduce FRD. One needs to make sure that all the conditions are the same (or scale these parameters to be the same) when comparing the performances of different fibers.

A mathematical model was derived that can be used to calculate the optimized fiber core size according to the required coupling efficiency. Extreme oversizing of the fiber core will reduce the IFU system performance. It was shown that the core radius should be between $d/2 + \sigma + \Delta t$ and $d/2 + 2\sigma + \Delta t$ in order to avoid extreme oversizing and light loss because of optical aberration and alignment error between the microlens and fiber.

A figure of merit for the IFU system was also derived, which can be used to compare and estimate the IFU performance. It was demonstrated that oversizing the fiber core and fiber FRD have the same effect on IFU performance.

REFERENCES

- Allington-Smith, J. R., & Content, R. 1998, *PASP*, 110, 1216
 Allington-Smith, J., et al. 2002, in *ASP Conf. Ser., Galaxies: The Third Dimension*, ed. M. Rosado, L. Binette, & L. Arias (San Francisco: ASP), in press (astro-ph/0202330)
 Anandarao, B. G., et al. 1983, *Proc. SPIE*, 445, 42
 Arribas, S., et al. 1998, in *ASP Conf. Ser. 152, Fiber Optics in Astronomy III*, ed. S. Arribas, E. Mediavilla, & F. Watson (San Francisco: ASP), 213
 Atherton, P. D. 1983, *Proc. SPIE*, 445, 535
 Bacon, R., et al. 1995, *A&AS*, 113, 347
 ———. 2001, *MNRAS*, 326, 23
 Bershady, M. A., et al. 1998, in *ASP Conf. Ser. 152, Fiber Optics in Astronomy III*, ed. S. Arribas, E. Mediavilla, & F. Watson (San Francisco: ASP), 253
 Boulesteix, J., et al. 1983, *Proc. SPIE*, 445, 37
 Bowen, I. S. 1938, *ApJ*, 88, 113
 Brodie, J. P., Lampton, M., & Bowyer, S. 1988, *AJ*, 96, 2005
 Carrasco, E., & Parry, I. 1994, *MNRAS*, 271, 1
 Connes, P. 1970, *ARA&A*, 8, 209
 Content, R. 1997, *Proc. SPIE*, 2871, 1295
 Content, R., & Allington-Smith, J. R. 2000, in *ASP Conf. Ser. 207, NGST Science and Technology Exposition*, ed. E. P. Smith & K. S. Long (San Francisco: ASP), 326
 Courtès, G. 1982, in *IAU Colloq. 67, Instrumentation for Astronomy with Large Optical Telescopes*, ed. C. M. Humphries (Dordrecht: Reidel), 123
 Dubbeldam, M., Content, R., Allington-Smith, J. R., Pokrovski, S., & Robertson, D. J. 2000, *Proc. SPIE*, 4008, 1181
 Gambling, W. A., Payne, D. N., & Matsumura, H. 1975, *Appl. Opt.*, 14, 1538
 Gloge, D. 1972, *Bell Syst. Tech. J.*, 51, 1767
 Guérin, J. 1998, in *ASP Conf. Ser. 152, Fiber Optics in Astronomy III*, ed. S. Arribas, E. Mediavilla, & F. Watson (San Francisco: ASP), 282
 Hailash, C. S., et al. 1983, *Proc. SPIE*, 445, 33
 Hall, D. N. B., Ridgway, S., Bell, E. A., & Yarborough, J. M. 1979, *Proc. SPIE*, 172, 121
 Haynes, R., & Allington-Smith, J. R. 1998, in *ASP Conf. Ser. 152, Fiber Optics in Astronomy III*, ed. S. Arribas, E. Mediavilla, & F. Watson (San Francisco: ASP), 289
 Haynes, R., Baldry, I. K., Taylor, K., & Lee, D. 2000, *Proc. SPIE*, 4008, 1203
 Heacock, W. D. 1986, *AJ*, 92, 219
 Herbst, T. M. 1998, *Proc. SPIE*, 3354, 720
 Herpe, G., Sanchez del Rio, J., Vanerriest, C., & del Olmo, A. 1998, in *ASP Conf. Ser. 152, Fiber Optics in Astronomy III*, ed. S. Arribas, E. Mediavilla, & F. Watson (San Francisco: ASP), 213
 Hill, J. M., & Angel, J. R. P. 1983, *Proc. SPIE*, 445, 85
 Jacobs, E. L., & Edwards, T. C. 1999, *Opt. Eng.*, 38, 827
 Jacquinet, P. 1954, *J. Opt. Soc. Am.*, 44, 761
 Lee, D., Haynes, R., Ren, D., & Allington-Smith, J. R. 2001, *PASP*, 113, 1406
 Maihara, T., et al. 2000, *Proc. SPIE*, 4008, 1111
 Maillard, J. P., & Michel, G. 1982, in *IAU Colloq. 67, Instrumentation for Astronomy with Large Optical Telescopes*, ed. C. M. Humphries (Dordrecht: Reidel), 213
 McGregor, P. J., Conroy, P., Bloxham, G., & van Harmelen, J. 1999, *Publ. Astron. Soc. Australia*, 16, 273
 McLean, I. 1997, *Electronic Imaging in Astronomy* (New York: Wiley)
 Murphy, T. W., Jr., Matthews, K., & Soifer, B. T. 1999, *PASP*, 111, 1176
 Nicia, A. 1981, *Appl. Opt.*, 20, 3136
 Parry, I. 1998, in *ASP Conf. Ser. 152, Fiber Optics in Astronomy III*, ed. S. Arribas, E. Mediavilla, & F. Watson (San Francisco: ASP), 3
 Parry, I., Kenworthy, M., & Taylor, K. 1997, *Proc. SPIE*, 2871, 1325
 Pierce, A. K. 1965, *PASP*, 77, 216

- Prieto, E., Le Fevre, O., Saisse, M., Hill, L., Voet, C., Mancini, D., Maccagni, D., Picat, J. P., & Vettolani, G. 1998, in ASP Conf. Ser. 152, *Fiber Optics in Astronomy III*, ed. S. Arribas, E. Mediavilla, & F. Watson (San Francisco: ASP), 229
- Ren, D. 2001, Ph.D. thesis, Univ. Durham
- Ridgway, S. H., & Brault, J. W. 1984, *ARA&A*, 22, 291
- Simons, D. A., Clark, C. C., Smith, S. S., Kerr, J. M., Massey, S., & Maillard, J.-P. 1997, *Proc. SPIE*, 2198, 185
- Sugai, H., et al. 2000, *Proc. SPIE*, 4008, 558
- Tecza, M., & Thatte, N. 1998, in ASP Conf. Ser. 152, *Fiber Optics in Astronomy III*, ed. S. Arribas, E. Mediavilla, & F. Watson (San Francisco: ASP), 271
- Vanderriest, C. 1980, *PASP*, 92, 858
- . 1998, in ASP Conf. Ser. 152, *Fiber Optics in Astronomy III*, ed. S. Arribas, E. Mediavilla, & F. Watson (San Francisco: ASP), 123
- Wade, R. 1983, *Proc. SPIE*, 445, 47
- Weitzel, L., Krabbe, A., Kroker, H., Thatte, N., Tacconi-Garman, L. E., Cameron, M., & Genzel, R. 1996, *A&AS*, 119, 531
- Wright, G. S., et al. 2000, *Proc. SPIE*, 4008, 729